

Steady streaming flows in viscoelastic liquids

Giridar Vishwanathan, Gabriel Juarez*

Department of Mechanical Science and Engineering, University of Illinois at Urbana-Champaign, Urbana, Illinois, 61801, USA

Abstract

We discuss experimental investigations on steady streaming flows of dilute and semi-dilute polymer solutions in microfluidic devices. The effect of non-Newtonian behavior on steady streaming for different model fluids is determined by characterizing the evolution of the inner streaming layer as a function of oscillation frequency using particle tracking velocimetry. We find that steady streaming velocity profiles in constant-viscosity elastic liquids are qualitatively similar to those in Newtonian liquids. Steady streaming velocity profiles in elastic liquids with strong shear thinning, however, display two unique features: (i) a non-monotonic evolution of the inner streaming layer with increasing frequency, first growing then decreasing in width, and (ii) a clear asymmetry in the flow profile at high frequencies.

Keywords: steady streaming, viscoelastic, microfluidics

Haiku

Endless vortices
A slippery solution
I see within them

1. Introduction

Steady streaming broadly refers to the steady, inertially rectified flow that occurs in the presence of a primary oscillatory flow [1, 2, 3]. The phenomenon of steady streaming is a viable tool for microfluidic applications ranging from particle sorting [4, 5], mixing [6, 7, 8], and trapping [9, 10, 11, 12]. Therefore, there is considerable interest in applying these flows to biological systems as a purely hydrodynamic method of manipulation [13, 14]. While non-Newtonian liquids are frequently encountered in biological systems, steady streaming in non-Newtonian liquids remains poorly understood, particularly in the context of micro-scale flows where there is maximum potential for application.

The classical problem of steady streaming around a cylinder of size a , oscillating with a frequency f , or angular frequency $\omega = 2\pi f$, and a far-field amplitude s in a Newtonian liquid is theoretically well-understood [3, 15, 16, 17], and thus provides a convenient baseline for studying steady streaming in non-Newtonian liquids. For a Newtonian liquid of kinematic viscosity ν , the streaming flow around a cylinder is caused by the rectified advection of vorticity from the curved surface. The streaming flow field typically manifests as two distinctly separated layers having four-fold symmetry with four vortices in each. The streamlines in the inner, viscous driving layer depend

only on the Stokes boundary layer width ($\sqrt{\nu/\omega}$) for a particular cylinder. The vortices in the outer, inertially driven layer rotate in the opposite sense and the flow profile is determined by the distance to the outer boundary. The inner layer grows with decreasing frequency and becomes very large when $\sqrt{\nu/\omega} \sim a$ [18]. The pathlines in both layers are independent of oscillation amplitude provided it is small, that is, $s/a \ll 1$. The streaming velocity, however, scales uniformly in magnitude with the oscillation amplitude as s^2 .

Dramatic changes in the steady streaming flow field of dilute polymer solutions around a cylinder oscillating at low frequencies ($10 \leq f \leq 100$ Hz) were experimentally observed [19]. In contrast to the Newtonian case, the inner streaming layer in non-Newtonian liquids was found to grow in size with increasing frequency, eventually displacing the outer driven vortices completely and giving the appearance of a reversed flow [20]. The growth of the inner streaming layer was theoretically described using viscoelastic constitutive models [21, 22, 23, 24], however, few studies have investigated the link between the steady streaming flow and the measured rheological properties of non-Newtonian liquids. One such study used steady streaming as a rheological tool to characterize drag-reduction in dilute polymer solutions [25]. While a qualitative correlation between the drag reduction performance and the liquid relaxation time was observed, inconsistencies in the measured relaxation times from steady streaming differed by two orders of magnitude when compared to estimates from steady shear rheology. This key observation implied that the longest relaxation time may not be the important characteristic time when considering steady streaming in non-Newtonian liquids.

The effectiveness of steady streaming as a microrheological tool has been reconsidered recently and demonstrated for low-viscosity Newtonian liquids in microfluidic devices [26]. In this work, we experimentally investigate steady streaming of

*Corresponding author

Email address: gjuarez@illinois.edu (Gabriel Juarez)

non-Newtonian liquids in microfluidic devices. A major advantage of the microscale approach is that higher frequencies can be accessed due to lower system inertia arising from small length scales $O(100 \mu\text{m})$. Further, smaller cylinder radii enable larger strains and improved spatial-temporal resolution of the rotational inner layer where the liquid rheology is critical, even though comparatively higher frequencies are used. The motivation for our study is three-fold. First, to make quantitative observations on the inner streaming layer of non-Newtonian liquids in the context of microfluidics where they stand to be most likely encountered in contemporary applications. Second, to explore the relationship between the bulk rheology and molecular properties of model dilute and semi-dilute polymer solutions with the observed streaming flows, and third, to elucidate the possible mechanism by which the non-Newtonian behavior manifests in streaming.

2. Experimental methods

2.1. Microfluidic steady streaming

Experiments were performed in microfluidic devices molded in PDMS, consisting of a straight channel 20 mm long, 5 mm wide, and 200 μm tall. A fixed cylindrical post with radius of $a = 100 \mu\text{m}$ was manufactured at the center of the straight channel. An oscillatory flow field, $U(t) = s\omega \cos(\omega t)$, was setup in the channel through an external oscillating pressure signal generated using an electro-acoustic transducer, or loudspeaker, over a range of frequencies, $50 \leq f \leq 1000 \text{ Hz}$. The oscillation amplitude was independently controlled over a range, $5 < s < 50 \mu\text{m}$, such that the non-dimensional amplitude ($\epsilon = s/a \ll 1$) is small. For a given data set, the value of $\epsilon^2\omega$ was maintained constant within $\pm 20\%$ of a mean value which lies in a range of 60 – 180 rad s^{-1} , depending on the viscosity of the liquid used. Note that $\epsilon^2\omega$ must be large enough for the streaming velocity to be unaffected by Brownian diffusion, and small enough that $\epsilon < 0.5$, even at the lowest frequency. The corresponding maximum streaming velocities measured for this range of $\epsilon^2\omega$ is between 50 – 500 $\mu\text{m/s}$, for a particular data set. The Reynolds number, $\text{Re} = \omega a^2/\nu$, and the streaming Reynolds number, $\text{Re}_s = \omega s^2/\nu$, correspond to a range of $2 \leq \text{Re} \leq 50$ and $0.1 \leq \text{Re}_s \leq 1$, respectively, for deionized water ($\nu = 0.949 \times 10^{-6} \text{ m}^2/\text{s}$) over the entire frequency range investigated here. This range of Re results in an inner streaming layer that is large compared to the cylinder radius and enables high resolution velocimetry of the inner layer.

Polystyrene tracer particles, 0.93 μm in diameter, were observed at the mid-height of the straight channel using bright field microscopy at 20 \times magnification (depth of focus $\approx 3 \mu\text{m}$). Images were acquired using a scientific CMOS camera where the sampling frequencies are much greater than (high-speed), or perfect divisors (stroboscopic) of the oscillatory flow frequency. High-speed imaging provided high fidelity observation of the oscillatory flow component and measurement of the oscillation amplitude s , while stroboscopic imaging was used to measure the streaming velocity fields. Experiments were performed at room temperature, maintained at 20 $^\circ\text{C}$.

2.2. Polymer solutions

Solutions were prepared by step-wise dissolution of different polymers into deionized (DI) water with gentle agitation at 60 rpm for 4 – 6 hours. After initial dispersion, the required final concentration was achieved by successive dilution with DI water. The polymers used in this study were xanthan gum (XG, $2.7 \times 10^6 \text{ MW}$, Sigma Aldrich G1253), non-ionic polyacrylamide (PAA, $6 \times 10^6 \text{ MW}$, Polysciences 02806), and polyacrylamide-acrylate co-polymer with a 30% degree of hydrolysis (hPAA, $18 \times 10^6 \text{ MW}$, Polysciences 18522). In addition to the above aqueous solutions, salinated polyacrylamide-acrylate (hPAAs) was prepared by dissolving hPAA in 0.5 M NaCl solution. The properties of the polymer molecules and the polymer solutions are listed in Table 1. Estimates of the overlap concentration c^* for these model solutions have been reported in literature [27, 28, 29]. Here, all solution concentrations are reported in parts-per-million (ppm) by weight, that is, 1 ppm = 10^{-6} gram of solute per gram of solvent.

2.3. Bulk rheology

The steady shear viscosity (η) versus shear rate ($\dot{\gamma}$), and the storage (G') and loss (G'') moduli versus angular frequency (ω) for some polymer solutions are shown in Figure 1. We characterize all liquids using a temperature-controlled cone-and-plate geometry rheometer (strain-controlled Ares G2, TA Instruments) at 25 $^\circ\text{C}$. We find strong shear thinning in 1000 ppm xanthan gum (XG 1000) and 50 ppm polyacrylamide-acrylate (hPAA 50) solutions, shown in Figure 1(a). At lower concentration solutions of XG 400 and hPAA 20 (not shown), shear thinning behavior is decreased. Shear thinning is minimal for the 4000 ppm non-ionic polyacrylamide (PAA 4000) and 500 ppm salinated polyacrylamide-acrylate (hPAAs 500) solutions, which can be considered Boger fluids, or constant-viscosity elastic liquids [30, 31].

The steady shear viscosity for the solutions shown in Figure 1(a) are modelled using a Carreau model [32], determined by a zero-shear viscosity η_0 , infinite-shear viscosity η_∞ (here, assumed to be solvent viscosity), power-law thinning index n and a relaxation time λ_{Cr} . The dynamic moduli of PAA 4000

Table 1: Properties of the various polymer molecules and aqueous polymer solutions used in this study.

Polymer solution	M_w [MDa]	c^* [ppm]	c [ppm]	c/c^*
XG	2.7	1600	400	0.25
XG			1000	0.63
PAA	6	550	4000	7.3
hPAA	18	200	20	0.1
hPAA			50	0.25
hPAAs			500	2.5

Here, M_w is polymer molecular weight, c^* and c are overlap and solute concentrations, respectively.

Table 2: Rheological fit parameters used in this study

Carreau	η_0 [Pa s]	η_∞ [Pa s]	λ_{Cr} [s]	n	R^2
hPAA 50	0.119	0.001	4.96	1.51	0.993
XG 1000	0.26	0.001	3.37	1.48	0.988
hPAA 500	0.0028	0.001	0.074	1.15	0.996
PAA 4000	0.012	0.001	0.046	1.16	0.999
Maxwell	η_M [Pa s]	λ_M [s]			R^2
PAA 4000	0.013	0.019			0.987
hPAA 500	0.0026	0.046			0.973
FMM	\mathbb{V} [Pa s $^\alpha$]	\mathbb{G} [Pa s $^\beta$]	α	β	R^2
hPAA 50	0.071	0.22	0.75	0.27	0.991
XG 1000	0.23	0.39	0.86	0.34	0.996

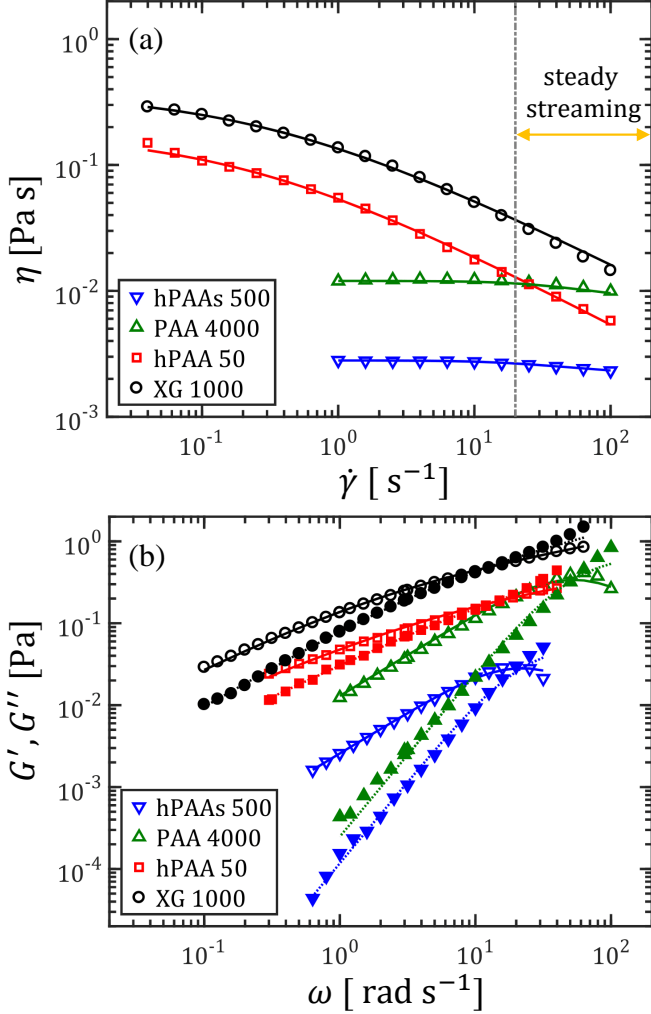


Figure 1: (a) Steady state shear viscosity measurements of dilute and semi-dilute polymer solutions used in this study and respective fits (solid line). The yellow arrow shows the mean range of shear rates encountered in experiments. (b) Storage (closed symbols) and loss (open symbols) moduli from oscillatory shear rheology of polymer solutions and model fits shown as solid and dashed lines, respectively. The model parameters used are listed in Table 2.

The table shows the model parameters used to obtain the fits shown in Figure 1. R^2 is a residual quantifying the agreement between the fit and the experimental data.

and hPAA 500 shown in Figure 1(b) are described well by the Maxwell model [32] and characterized by a viscosity η_M , and relaxation time λ_M . The dynamic moduli for XG 1000 and hPAA 50 on the other hand, are modelled well using a fractional Maxwell model (FMM) [33] described by two dimensionless exponents: $0 \leq \beta \leq 0.5$ and $\beta \leq \alpha \leq 1$; along with two stiffness quasi-properties \mathbb{G} and \mathbb{V} . The model based fits are shown in Figure 1 as solid or dashed lines, while the model parameters are listed in Table 2.

A relaxation time can also be inferred from the crossover angular frequency (ω_{co}) at which the storage and loss moduli are equal and determined by $\lambda_{co} = 1/\omega_{co}$. A more rigorous estimate of the relaxation time from the model parameters are $\lambda_M \approx \lambda_{co}$ for a Maxwell liquid and $\lambda_{FMM} = (\mathbb{V}/\mathbb{G})^{1/(\alpha-\beta)}$ for a fractional Maxwell liquid. Yet another estimate of the relaxation time for the constant-viscosity polymer solutions (dilute and semi-dilute unentangled) can be obtained from molecular

Table 3: Relaxation time estimates from different models

Polymer solution	λ_Z [ms]	λ_{co} [ms]	λ_{Cr} [ms]	λ_{FMM} [ms]
XG 1000	-	79	3370	362
PAA 4000	2.7	17	46	-
hPAA 50	-	83	4960	94.7
hPAA 500	11.2	50	74	-

Above, λ_Z is from Zimm theory, λ_{co} is from the crossover of dynamic moduli, λ_{Cr} is from the Carreau model, and λ_{FMM} is from the fractional Maxwell model. The relaxation times may be compared to $\lambda_{ref} = 0.4$ ms, for which $\lambda_{ref}\omega = 1$ at 400 Hz.

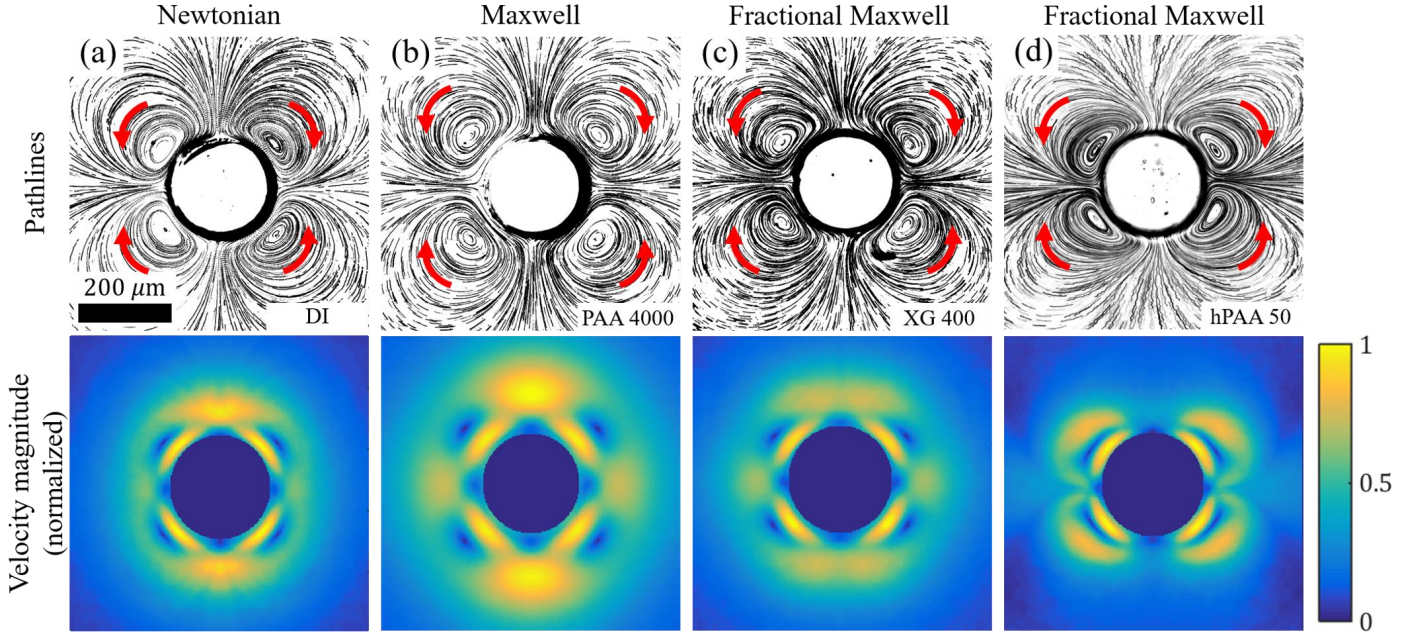


Figure 2: Steady streaming profiles in Newtonian and non-Newtonian liquids at an oscillation frequency of 600 Hz around a cylinder with radius of $100 \mu\text{m}$. (Top row) Pathlines of tracer particles for (a) DI water and $\epsilon = 0.07$, (b) 4000 ppm non-ionic polyacrylamide and $\epsilon = 0.08$, (c) 400 ppm xanthan gum and $\epsilon = 0.15$, and (d) 50 ppm hydrolyzed polyacrylamide and $\epsilon = 0.19$. (Bottom row) Corresponding steady streaming velocity magnitude field, normalized by the maximum streaming velocity, obtained from particle tracking velocimetry. High-velocity regions, light (or yellow) regions of the colormap, are located near the cylinder boundary.

considerations using the Zimm formula [34]:

$$\lambda_z = \frac{\eta_s [\eta]_0 M_w}{2.37RT}, \quad (1)$$

where η_s is the solvent viscosity, $[\eta]_0$ is the intrinsic shear viscosity at zero shear rate, R is the universal gas constant, and T is the temperature. Here, we take $\eta_s = \eta_\infty = 1 \times 10^{-3} \text{ Pa s}$ (DI water) and $[\eta]_0$ was approximated for the solutions used based on the zero-shear viscosity and solvent viscosity. The various estimates of relaxation times from the different methods are listed in Table 3. Note that the Zimm theory cannot be applied to polyelectrolyte solutions such as XG and hPAA in the absence of salts [28].

3. Results

The comparison between steady streaming in Newtonian and non-Newtonian liquids at an oscillation frequency of 600 Hz is shown in Figure 2. The particle pathlines (top row) are generated from minimum intensity projections of a sequence of stroboscopic images and the velocity magnitude fields (bottom row) are obtained from particle tracking velocimetry. For all cases, the quadrupolar topology of the streaming flow field is preserved, consisting of four identical vortices with distinct centers. Similarly, the rectified flow moves toward the cylinder along the axis of oscillation and away from the cylinder normal to the axis of oscillation.

The pathlines and velocity magnitude field for a Newtonian liquid, deionized water, are shown in Figure 2(a, top and bottom). High flow velocities are located in the regions between the cylinder surface and the eddy center, and near the cylinder

surface, perpendicular to the axis of oscillation. This latter difference, compared to the velocity along the axis, is because of increased interaction with the channel wall in the breadthwise direction as compared to the lengthwise direction.

The steady streaming pathlines and velocity magnitude field of a Maxwell liquid, PAA 4000, are qualitatively similar to that of a Newtonian liquid, shown in Figure 2(b, top and bottom). The main difference, compared with DI water, is the eddy center distance from the cylinder surface, which is larger for PAA 4000. This larger eddy center distance indicates a higher viscosity for PAA 4000, as was recently demonstrated [26], and is in agreement with steady state shear viscosity measurements shown in Figure 1(a).

In the fractional Maxwell liquids, a qualitative difference is observed in particle pathlines and velocity magnitude fields. For XG 400 solutions, the angular position of the eddy centers move closer to the axis of oscillation, shown in Figure 2(c, top). The velocity field has also observably changed with the velocity maximum, normal to the axis of oscillation, separated into two regions by a local minimum, shown in Figure 2(c, bottom). For hPAA 50 solutions, a more prominent change is seen where the angular position of the eddy center as well as the velocity maximum are moved considerably towards the axis of oscillation, Figure 2(d, top and bottom).

To quantify differences in the steady streaming profile for various liquids over a range of frequencies, the normalized tangential velocity profile as a function of the dimensionless radial position (r/a) along a transect from the cylinder surface through the eddy center was examined. The transect is depicted by the red dashed arrow passing through the eddy center in Fig-

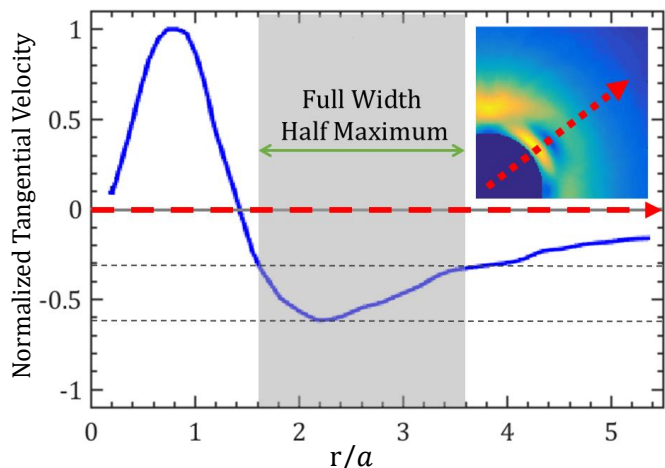


Figure 3: Representative steady streaming tangential velocity profile, normalized by the maximum streaming velocity, as a function of dimensionless radial position. This profile is taken along the transect starting from the cylinder surface and radially outward through the eddy center, as shown in the inset. The velocity is highest in magnitude near the cylinder surface and zero at the eddy center location, as it goes from positive to negative values. The full width at half maximum (FWHM) of the second (negative) peak is used to characterize the width of the inner layer and is annotated for DI water at an oscillation frequency of 100 Hz.

ure 3(inset). A representative experimentally measured velocity profile for a Newtonian liquid is shown in Figure 3. The particular parameter of interest is the full width at half maximum (FWHM) of the second peak, beyond the eddy center. The FWHM provides a measure of the size of the inner layer in this streaming regime where a distinctly visible separation between the inner and outer layers is absent. The FWHM is also preferred because of the insensitivity to inaccuracies in particle tracking close to the cylinder surface as well as inaccuracies in the measurement of oscillation amplitude (s).

The variation of the FWHM with frequency for Newtonian liquids, DI water and aqueous 60% glycerol (w/w) with a dynamic viscosity of 5.9 mPa s, and Maxwell liquids, PAA 4000 and hPAAs 500, is shown in Figure 4(a). The Newtonian liquids exhibit slow monotonic decrease in the FWHM with increasing oscillation frequency. The Maxwell liquids show a nominally faster rate of decrease in the FWHM with increasing frequency, without any discernible features.

This is in sharp contrast with the observations for fractional Maxwell liquids. All four polymer solutions exhibit distinct peaks in their FWHM with increasing oscillation frequency, shown in Figure 4(b). For hPAA 50 ppm solutions, the FWHM grows rapidly for oscillation frequencies of 75 Hz to 150 Hz, which is in agreement with previous observations [25]. However, the FWHM begins to decrease with further increasing frequency until its variation is similar to that of the solvent. Similar trends are observed for hPAA 20 solutions, with the maximum FWHM observed at 75 Hz and a subsequent rapid decrease to Newtonian-like behavior.

The XG 1000 and XG 400 solutions also behave in a manner consistent with our observations for the hPAA solutions, exhibiting a distinct peak in the FWHM followed by a decrease

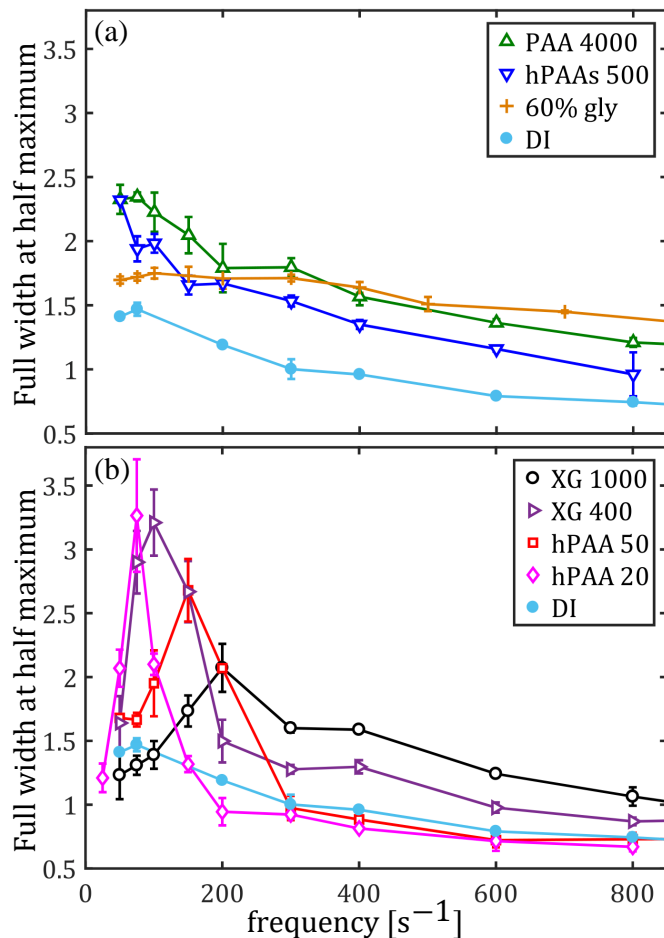


Figure 4: Evolution of inner streaming layer characterized by the full width at half maximum for Newtonian and non-Newtonian liquids as a function of oscillation frequency in microfluidic devices. (a) The FWHM of Newtonian liquids and Maxwell liquids exhibit monotonic decrease with increasing oscillation frequency. (b) The FWHM of fractional Maxwell liquids, however, increases to a maximum value and then decreases with increasing oscillation frequency.

to Newtonian-like behavior with increasing frequency. The key difference between the two polymers is the rate at which they decrease at large frequencies, which is slower for XG solutions. This is in agreement with the qualitative observations where the pathlines and the corresponding velocity magnitude fields are not as distorted in XG as they are in hPAA, even at 600 Hz, shown in Figure 2(c) and (d). Further increase in frequency is not found to significantly alter the velocity profile of hPAA 20 and hPAA 50 solutions, while XG 400 shows a gradual approach towards velocity fields similar to those of hPAA 50. This approach is slower still for XG 1000 and therefore reflected completely by the evolution of the FWHM shown in Figure 4.

4. Discussion

The significant departure from four-fold symmetry in the streaming flow profile observed for Fractional Maxwell liquids, as compared to the Newtonian case in Figure 2(top), is attributed to the nature of the oscillatory strain field and the shear thinning rheology of these liquids (see Figure 1(a)). At leading order, the rate of strain ($O(\epsilon\omega)$) in the vicinity of the cylinder is completely extensional along the axis of oscillation, and purely shearing perpendicular to it. The spatial-temporal mean rates of extension and shear obtained theoretically [16] for DI water with $\nu = 10^{-6}$ m²/s and a cylinder radius of 100 μ m are $0.15\epsilon\omega$ and $0.45\epsilon\omega$, respectively. For the frequencies used in this study, the mean strain rates are in the range $50 - 200$ s⁻¹ for shear (shown in Figure 1(a)) and $15 - 60$ s⁻¹ in the case of extension. The corresponding maximum, instantaneous rates of extension and shear are $0.3\epsilon\omega$ and $3.73\epsilon\omega$, respectively. The relatively large prefactor for shear is due to its localization near the cylinder surface. As a result, the effective viscosity is considerably lower in the high shear region for liquids exhibiting shear thinning, and consequently asymmetry is observed in the streaming flow profile. Maxwell liquids, on the other hand, exhibit minimal shear thinning behavior in this range of shear rates. Therefore, the location of the eddy center and overall streaming flow profile does not differ significantly in comparison to Newtonian liquids.

The growth of the inner streaming layer for a cylinder oscillating at frequencies $f < 100$ Hz in dilute hydrolyzed polyacrylamide solutions has been experimentally observed [25]. Although the growth of the inner layer at unity Deborah numbers ($De = \lambda\omega \approx 1$) was analytically understood to be an effect of elasticity using viscoelastic models [21, 23, 22], the most relevant estimate of the relaxation time remains ambiguous. Different estimates of relaxation time for liquids such as hPAA 50 and XG 1000 that show inner layer growth, are listed in Table 3. The estimates vary considerably depending on the rheology data used, all of which yield $De > 10$, even at 20 Hz.

In contrast, the experimental results presented here for Maxwell liquids indicate a decrease of the inner layer width, without the characteristic growth. While this observation is consistent with previous experiments, which report almost Newtonian behavior for similar liquids [25], we note that $De > 10$ even at 100 Hz, regardless of the relaxation time estimate

used from Table 3. This lack of inner layer growth is unsurprising when we consider that coil-stretch transitions are theorized to require $\epsilon\lambda_Z > 1$ in purely extensional flow [35, 36]. Estimating the maximum instantaneous rate of extension in our experiments ($\epsilon \leq 0.3\epsilon\omega$) to be $30 - 100$ s⁻¹, the values of λ_Z shown in Table 3 do not satisfy the criterion. Hence, polymer stretching in the primary flow is likely insufficient for the growth of the inner streaming layer in Maxwell liquids.

The decrease of the inner layer width following the initial growth in the fractional Maxwell liquids has not been reported before and is best explained by a competition between the effects of inertia and elasticity. This competition was suggested in the theoretical analysis for an oscillating sphere (see Fig. 4 and Fig. 6 in Ref. [24]) and quantified through the material functions $S = \rho a^2 \omega^2 / G''$ and $V = G' / G''$, which are analogs of the Reynolds number and Deborah number, respectively. Similar to theories for a cylinder, increasing V while keeping S fixed was found to increase the width of the inner streaming layer. Increasing S for a fixed V , however, results in a set of cascading same sense vortices, of which, the innermost vortex decreases in width. Owing to the dependence of both S and V on ω , it is difficult to experimentally achieve independent control.

Regardless, the first experimental evidence of cascading same sense vortices for a fractional Maxwell liquid (hPAA 50) at 800 Hz is shown in Figure 5. An important implication of this observation is that, eventually, the effect of a growing S dominates over that of a growing V . Indeed, we find that this is the case from Figure 6 which shows the variation of the material functions S and V with frequency for the models and fit parameters given in Table 2. The values to the left of the vertical dotted line lie in the range of frequencies for which the oscillatory rheology was measured while those to the right are an extrapolation and lie in the frequency range for which streaming is studied.

For fractional Maxwell liquids (dotted lines) and frequencies $f > 100$ Hz, V saturates in the range of $1.5 < V < 2$ while S grows much faster to $10 < S < 100$. Therefore, there is quantitative concord with our experimental observations of growth and subsequent shrinking of the inner layer beyond ($V = 1.5, S = 50$), and the corresponding values of ($V = 2, S = 50$) shown elsewhere [24] at which the cascading vortices manifest, albeit for a sphere. This suggests that a description of viscoelasticity in terms of S and V is more robust than one based on relaxation times.

For the Maxwell liquids, however, the material function V increases rapidly when extrapolated to frequencies $f > 20$ Hz (solid lines in Figure 6(bottom)). Notwithstanding that the polymer chains are likely insufficiently stretched in the flow, it is worth noting that rapid growth of V for a Maxwell liquid is unphysical because it requires an indefinitely decreasing G'' for an approximately constant G' . The solvent viscosity (here $\eta_\infty = 1$ mPa.s) provides a definite lower bound on the loss modulus, and hence, an upper bound for V given by $G' / (\eta_\infty \omega)$ and shown in Figure 6(bottom, dashed lines). Thus, for the Maxwell liquids, an increasing ω will eventually lead to a decrease in V or, at least, a significant decrease in its growth with frequency. This is also true of S for which is limited by the corresponding

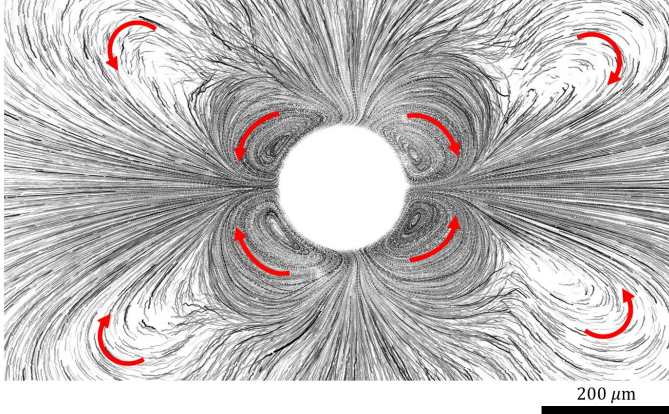


Figure 5: Pathlines of tracer particles illustrating experimental evidence of the predicted cascading inertio-elastic vortices. A set of secondary, same-sense vortices is shown for an hPAA 50 polymer solution at an oscillation frequency of 800 Hz and non-dimensional amplitude of $\epsilon = 0.2$.

curve for DI water (top, dashed lines).

5. Conclusions

In this experimental work, we have studied the inner steady streaming layer of dilute and semi-dilute polymer solutions, having both Maxwell and fractional Maxwell oscillatory shear rheology. Qualitative differences in the velocity fields are observed for fractional Maxwell liquids, most prominently, an angular displacement of the eddy centers towards the direction of oscillation and consequent asymmetry. The width of the inner streaming layer is characterized by the full width at half maximum of the velocity profile along the eddy center from the cylinder boundary. We find that the inner streaming layer width of fractional Maxwell liquids exhibits a non-monotonic relationship with oscillation frequency; first increasing in width followed by a decrease in width with increasing frequency. This behavior is attributed to a competition between elasticity and inertia, with inertia dominating at high frequencies. Maxwell liquids, however, exhibit a monotonic decrease of the inner streaming layer width with increasing frequency at a rate nominally faster than that observed for a Newtonian liquid. Even for oscillation periods considerably smaller than the molecular relaxation time, we do not observe any qualitative change in the flow profile as compared to a Newtonian liquid. This behavior is attributed to the insufficient molecular stretching by the underlying oscillatory flow.

6. Acknowledgments

We thank Gwynn J. Elfring and Saverio E. Spagnolie for the invitation to present preliminary results of this work at the Banff International Research Station “Complex Fluids in Biological Systems” workshop. We also thank Luca Martinetti for steady shear and oscillatory shear rheology measurements.

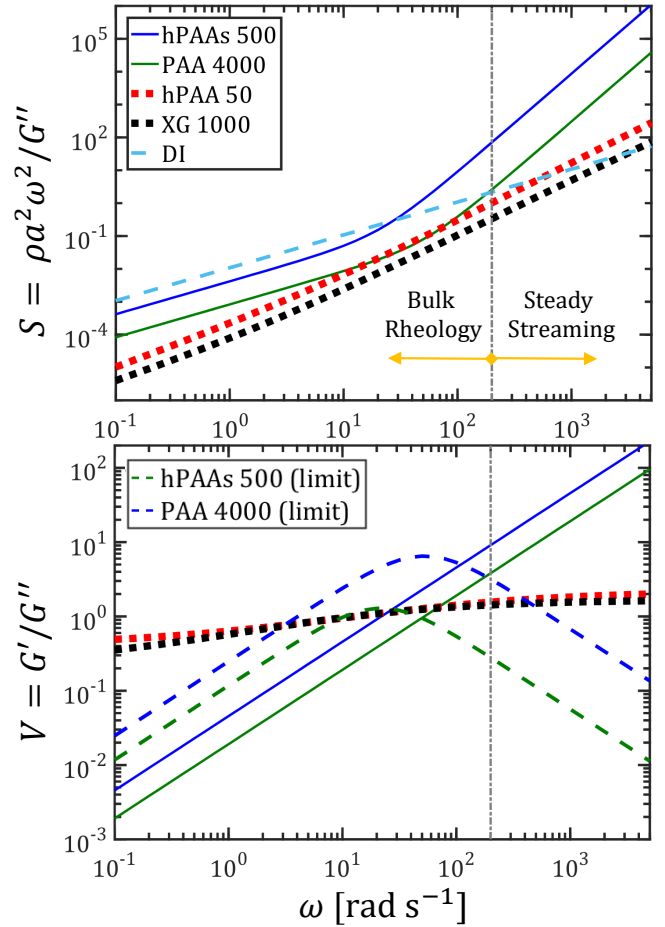


Figure 6: Variation of S (top) and V (bottom) with angular frequency based on the rheology fit models. Oscillatory rheology was performed in the frequency range to the left of the vertical line while streaming experiments were performed in the range of frequencies to the right.

References

References

- [1] E. N. da C. Andrade, On the circulations caused by the vibration of air in a tube, *Proceedings of the Royal Society A: Mathematical, Physical and Engineering Sciences* 824 (1931) 445–470.
- [2] N. Riley, *Encyclopedia of Acoustics*, Wiley, 1997, Ch. Acoustic streaming, pp. 321–327.
- [3] N. Riley, Steady streaming, *Annual Review of Fluid Mechanics* 33 (2001) 43–65.
- [4] C. Wang, S. V. Jalikop, S. Hilgenfeldt, Size-sensitive sorting of microparticles through control of flow geometry, *Applied Physics Letters* 99 (2011) 034101.
- [5] R. Thameem, B. Rallabandi, S. Hilgenfeldt, Fast inertial particle manipulation in oscillating flows, *Physical Review Fluids* 2 (2017) 052001.
- [6] K. Sritharan, C. J. Strobl, M. F. Schneider, A. Wixforth, Z. Guttenberg, Acoustic mixing at low Reynolds numbers, *Applied Physics Letters* 88 (2006) 054102.
- [7] B. R. Lutz, J. Chen, D. T. Schwartz, Characterizing homogeneous chemistry using well-mixed microeddies, *Analytical Chemistry* 78 (2006) 1606–1612.
- [8] D. Ahmed, X. Mao, J. Shi, B. K. Juluri, T. J. Huang, A millisecond micromixer via single-bubble-based acoustic streaming, *Lab on Chip* 9 (2009) 2738–2741.
- [9] P. Marmottant, S. Hilgenfeldt, Controlled vesicle deformation and lysis by single oscillating bubbles, *Nature* 423 (2003) 153–156.
- [10] B. R. Lutz, J. Chen, D. D. T. Schwartz, Hydrodynamic tweezers: 1. non-contact trapping of single cells using steady streaming microeddies, *Analytical Chemistry* 78 (2006) 5429–5435.
- [11] V. H. Lieu, T. A. House, D. T. Schwartz, Hydrodynamic tweezers: Impact of design geometry on flow and microparticle trapping, *Analytical Chemistry* 84.
- [12] S. Yazdi, A. M. Ardekani, Bacterial aggregation and biofilm formation in a vortical flow, *Biomicrofluidics* 6 (2012) 044114.
- [13] M. Wiklund, R. Green, M. Ohlin, *Acoustofluidics 14: Applications of acoustic streaming in microfluidic devices*, *Lab on a Chip* 12 (2012) 2438–2451.
- [14] J. Friend, L. Y. Yeo, Microscale acoustofluidics: Microfluidics driven via acoustics and ultrasonics, *Reviews of Modern Physics* 83 (2011) 647–704.
- [15] C.-Y. Wang, On high-frequency oscillatory viscous flows, *Journal of Fluid Mechanics* 32 (1968) 55–68.
- [16] J. Holtmark, I. Johnsen, T. Sikkeland, S. Skavlem, Boundary layer flow near a cylindrical obstacle in an oscillating, incompressible fluid, *The Journal of the Acoustical Society of America* 26 (1954) 26.
- [17] A. F. Bertelsen, An experimental investigation of high Reynolds number steady streaming generated by oscillating cylinders, *Journal of Fluid Mechanics* 64 (1974) 589598.
- [18] W. P. Raney, J. C. Corelli, P. J. Westervelt, Acoustical streaming in the vicinity of a cylinder, *The Journal of the Acoustical Society of America* 26 (1954) 1006–1014.
- [19] C. Chang, W. R. Schowalter, Flow near and oscillating cylinder in dilute viscoelastic fluid, *Nature* 252 (1974) 686–688.
- [20] C. Chang, W. R. Schowalter, Secondary flow in the neighborhood of a cylinder oscillating in a viscoelastic fluid, *Journal of Non-Newtonian Fluid Mechanics* 6 (1979) 47–67.
- [21] K. R. Frater, Acoustic streaming in an elastico-viscous fluid, *Journal of Fluid Mechanics* 30 (4) (1967) 689697.
- [22] C. Chang, Boundary layer analysis of oscillating cylinder flows in a viscoelastic liquid, *Journal of Applied Mathematics and Physics* 28 (1977) 283–288.
- [23] P. W. James, Elastico-viscous flow around a circular cylinder executing small amplitude, high frequency oscillations, *Journal of Non-Newtonian Fluid Mechanics* 2 (1977) 99–107.
- [24] G. Böhme, On streaming in viscoelastic liquids, *Journal of Non-Newtonian Fluid Mechanics* 44 (1992) 149–170.
- [25] D. Vlassopoulos, W. R. Schowalter, Characterization of the non-Newtonian flow behavior of drag-reducing fluids, *Journal of Non-Newtonian Fluid Mechanics* 49 (1993) 205–250.
- [26] G. Vishwanathan, G. Juarez, Steady streaming viscometry of Newtonian liquids, *Physics of Fluids* 31 (2019) 041701.
- [27] W. M. Kulicke, R. Haas, Flow behavior of dilute polyacrylamide solutions through porous media. 1. influence of chain length, concentration, and thermodynamic quality of the solvent, *Industrial & Engineering Chemistry Fundamentals* 23 (3) (1984) 308–315.
- [28] E. Turkoz, A. Perazzo, C. Arnold, H. Stone, Salt type and concentration affect the viscoelasticity of polyelectrolyte solutions, *Applied Physics Letters* 112 (20).
- [29] J. François, D. Sarazin, T. Schwartz, G. Weill, Polyacrylamide in water: molecular weight dependence of $\langle R^2 \rangle$ and $[\eta]$ and the problem of the excluded volume exponent, *Polymer* 20 (8) (1979) 969 – 975.
- [30] D. V. Boger, A highly elastic constant-viscosity fluid, *Journal of Non-Newtonian Fluid Mechanics* 3 (1977/78) 87–91.
- [31] D. F. James, Boger fluids, *Annual Review of Fluid Mechanics* 41 (2009) 129–142.
- [32] R. B. Bird, R. C. Armstrong, O. Hassager, *Dynamics of Polymeric Liquids*. Vol. 1, 2nd Ed.: *Fluid Mechanics*, Wiley, 1987.
- [33] A. Jaishankar, G. H. McKinley, A fractional K-BKZ constitutive formulation for describing the nonlinear rheology of multiscale complex fluids, *Journal of Rheology* 58 (2014) 1751–1788.
- [34] B. H. Zimm, Dynamics of polymer molecules in dilute solution: Viscoelasticity, flow birefringence and dielectric loss, *The Journal of Chemical Physics* 24 (1956) 269–278.
- [35] P. G. de Gennes, Coilstretch transition of dilute flexible polymers under ultrahigh velocity gradients, *The Journal of Chemical Physics* 60 (12) (1974) 5030–5042.
- [36] R. G. Larson, J. J. Magda, Coil-stretch transitions in mixed shear and extensional flows of dilute polymer solutions, *Macromolecules* 22 (1989) 3004–3010.